

# On Using Deep Convolutional Neural Network Architectures for Object Classification and Detection within X-ray Baggage Security Imagery

Samet Akcay\*, Mikolaj E. Kundegorski, Chris G. Willcocks, and Toby P. Breckon

**Abstract**—We consider the use of deep Convolutional Neural Networks (CNN) with transfer learning for the image classification and detection problems posed within the context of X-ray baggage security imagery. The use of the CNN approach requires large amounts of data to facilitate a complex end-to-end feature extraction and classification process. Within the context of X-ray security screening, limited availability of object of interest data examples can thus pose a problem. To overcome this issue, we employ a transfer learning paradigm such that a pre-trained CNN, primarily trained for generalized image classification tasks where sufficient training data exists, can be optimized explicitly as a later secondary process towards this application domain. To provide a consistent feature-space comparison between this approach and traditional feature space representations, we also train Support Vector Machine (SVM) classifier on CNN features. We empirically show that fine-tuned CNN features yield superior performance to conventional hand-crafted features on object classification tasks within this context. Overall we achieve 0.994 accuracy based on AlexNet features trained with Support Vector Machine (SVM) classifier. In addition to classification, we also explore the applicability of multiple CNN driven detection paradigms such as sliding window based CNN (SW-CNN), Faster RCNN (F-RCNN), Region-based Fully Convolutional Networks (R-FCN) and YOLOv2. We train numerous networks tackling both single and multiple detections over SW-CNN/F-RCNN/R-FCN/YOLOv2 variants. YOLOv2, Faster-RCNN, and R-FCN provide superior results to the more traditional SW-CNN approaches. With the use of YOLOv2, using input images of size  $544 \times 544$ , we achieve 0.885 mean average precision (mAP) for a six-class object detection problem. The same approach with an input of size  $416 \times 416$  yields 0.974 mAP for the two-class firearm detection problem and requires approximately 100ms per image. Overall we illustrate the comparative performance of these techniques and show that object localization strategies cope well with cluttered X-ray security imagery where classification techniques fail.

**Index Terms**—Deep convolutional neural networks, transfer learning, image classification, detection, X-ray baggage security

## I. INTRODUCTION

**X**RAY baggage security screening is widely used to maintain aviation and transport security and poses a significant image-based screening task for human operators reviewing compact, cluttered and highly varying baggage contents within limited time-scales. The increased passenger throughput, in the global travel network, and the increased focus on broader aspects of extended border security (e.g., freight, shipping,

postal) results in a challenging and timely automated image classification task.



Fig. 1: Exemplar X-ray baggage imagery multiple objects.

Previous work within this context is primarily based on the bag of visual words model (BoVW) [1]–[5] although there is some limited research using other techniques such as sparse representations [6]. Convolutional neural networks (CNN), a state-of-the-art paradigm for contemporary computer vision problems, were introduced into the field of X-ray baggage imagery by [7], comparing CNN to a BoVW approach with conventional hand-crafted features trained with a Support Vector Machine (SVM) classifier. Following the work of [7], [8] also studies X-ray baggage object classification with CNN similarly comparing it against traditional classifiers.

Motivated by [4], [7], [8], we conduct an extensive set of experiments to evaluate the strength of CNN features and traditional hand-crafted features (SIFT, SURF, FAST, KAZE [4]). As with [7], we perform layer freezing by fixing parameters from the source domain without any further optimization to observe how fixing the layer parameters at varying points in the network influences the overall performance of the transfer learning based tuning of the end-to-end CNN. Furthermore, in contrast to [7], [8] comparing end-to-end CNN classification with traditional feature-driven pipelines, we additionally present results whereby we extract the output of the last layer of a given CNN ( $fc_7$  of AlexNet [9]) as a feature map itself. We subsequently train an SVM classifier, generally used as the final classification stage of feature-driven approaches [1]–[5], to provide a consistent feature-space comparison between both learned (CNN) and traditional feature representations.

In addition to the proposed classification scheme, we explore object detection within this problem domain by investigating both the use of a sliding window paradigm (akin to [5], [10]) and evaluate contemporary approaches to learn efficient object localization via R-CNN [11], R-FCN [12] and YOLOv2 [13] approaches. As shown in previous work [7], [8] the challenging and cluttered nature of object detection in X-ray security imagery often poses additional challenges

S.Akcay\*, C.G.Willcocks, T.P.Breckon are with Department of Computer Science, Durham University, Durham, UK (e-mail: { samet.akcay, christopher.g.willcocks, toby.breckon }@durham.ac.uk).

M.E.Kundegorski was with Department of Computer Science, Durham University, Durham, UK.

Asterisk indicates corresponding author.

for established contemporary classification and detection approaches, such as RCNN/R-FCN [11], [12].

The main contributions of this paper are: (a) the exhaustive evaluation of classification architectures of [9], [14]–[16] against prior work in the field from [1], [2], [4], [6], [17], (b) the feature-space comparison of the end-to-end CNN classification results of [7], [8] against the final stage SVM classification on the extracted CNN features, (c) the comparison of the region based object detection/localization strategies of [11], [12] against the prior strategies proposed in [10], [18]. Contrasting performance results are obtained against the prior published studies of [4], [7] over a comprehensive dataset of 11,627 examples making this the largest combined X-ray object detection and classification study in the literature to date. Moreover, the evaluation is strengthened further by using UK government evaluation dataset [19] (available upon request from UK Home Office Centre for Applied Science and Technology (CAST)). Overall, we identify classification approaches and detection strategies that outperform the prior work of [5], [7], [10].

## II. RELATED WORK

Aviation security screening systems are of interest and have been studied for decades [20]. Computer Aided Screening (CAS) performs automated threat detection in the generalized sense, however this largely remains an unsolved problem. Previous work [21], [22] has focused on image enhancement [23]–[25], segmentation [26], [27], classification [1], [2], [4], [6], [17] or detection [5], [10], [28], [29] tasks in order to further investigate the real time applicability of CAS to automatize aviation security screening. For a detailed overview the reader is directed to Rodgers *et al.* [22] and Mouton *et al.* [21]. Our focus is based on addressing the object classification and detection tasks presented in the following sections.

**Classification:** For the classification of X-ray objects, the majority of prior work proposes traditional machine learning approaches based on a Bag-of-Visual-Words (BoVW) feature representation scheme, using hand-crafted features together with a classifier such as a Support Vector Machine (SVM) [1], [2], [4], [6], [17].

The work of [1] considers the concept of BoVW within X-ray baggage imagery using SVM classification with several feature representations (DoG, DoG+SIFT, DoG+Harris) achieving a performance of 0.7 recall, 0.29 precision, and 0.57 average precision. Turcsany *et al.* [2] followed a similar approach and extended the work presented in [1]. Using a BoVW with SURF descriptors and an SVM classifier, together with a modified version of codebook generation, yields 0.99 true positive and 0.04 false positive rates [2]. BoVW approaches with feature descriptor and SVM classification are also used in [3] for the classification of single and dual-view X-ray images, with optimal average precisions achieved for firearms (0.95) and laptops (0.98). Mery *et al.* [17] propose a recognition approach that applies detection to single-view images to find objects of interest, and then matches these across multiple view X-ray images yielding 0.96 precision and 0.93 recall for 120 objects. A BoVW approach is further employed in [6] where

a dictionary is formed for each class that consists of feature descriptors of randomly cropped image patches. Performance of the model is evaluated by fitting a sparse representation classification to the extracted feature descriptors of randomly cropped test patches, and adaptive dictionaries are obtained from the training stage. The experimental procedure demonstrates promising results for classification of the patches.

Kundegorski *et al.* [4] exhaustively explore the use of various feature point descriptors as visual word variants within a BoVW model. This is for image classification based threat detection within baggage security X-ray imagery, using a FAST-SURF feature detector and descriptor combination giving a maximal performance with an SVM classification (2 class firearm detection: 94.0% accuracy).

The study of [7] compares a BoVW approach and a CNN approach, exploring the use of transfer learning by fine-tuning weights of different layers transferred from another network trained on a different task. Experiments show that the CNN outperforms the BoVW method, even when features are abstractly transferred from another classification problem. Following the earlier work of [7], [8] exhaustively explores the use of varying classification approaches within the X-ray baggage domain using ten different techniques, including BoVW, sparse representations, and CNN. Experiments show parallel results with [7], supporting the generalized superiority of CNN features but without any further consideration of the initial object detection (localization) problem, or exhaustive exploration of CNN performance in the broader sense.

**Detection:** Object classification is a significant task for the identification (semantic labeling) of particular objects against others, i.e., being a threat or non-threat. However, a vital remaining task within this problem domain is that of detection in which objects of interest are localized within the overall X-ray image, commonly denoted with a bounding box or shape outline. Since detection is a challenging problem, detection based models within X-ray baggage imagery are significantly more limited in the literature.

In [28], detection of regions of interest (ROI) within X-ray images is performed via a geometric model of the object, by estimating structure from motion. Potential regions obtained from segmentation step are then tracked based on their similarity, achieving 0.943 true positive and 0.056 false positive rates on a small, uncluttered dataset.

Franzel *et al.* [10] propose a sliding window detection approach with the use of a linear SVM classifier and histogram of oriented gradients (HOG) [31]. As HOG is not fully rotationally invariant, they supplement their approach by detection of varying orientations. As a next step, called multi-view integration, detections from single view X-ray images, taken from multiple viewpoints in a modern X-ray scanner machine, are fused to avoid false detections and find the intersection of the true detections. Multi-view detection is shown to provide superior detection performance to single-view detection for handguns (mAP: 0.645). Similarly, [5] explores object detection in X-ray baggage imagery by evaluating various hand-crafted feature detector and descriptor combinations with the use of a branch and bound algorithm and structural SVM classifier (mAP: 0.881 for 6400 images of handguns, laptops

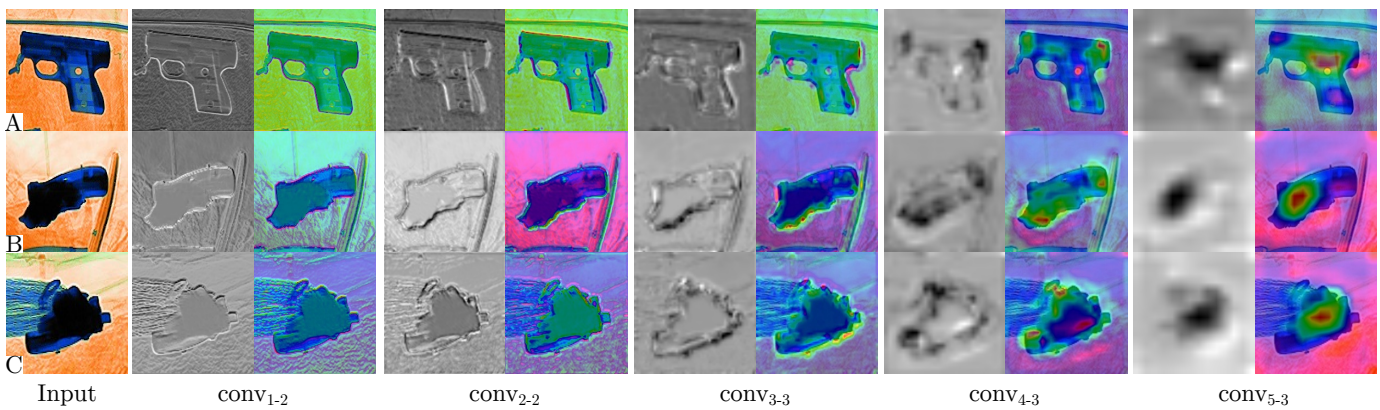


Fig. 2: Gradient-based class activation map (Grad-CAM [30]) of VGG16 [15] trained on X-ray data. The first column of each convolution box demonstrates grayscale Grad-CAM, while the second column is Grad-CAM heatmap on an input image.

and glass bottles).

A related body of work also targets the use of BoVW techniques within the highly related task object detection within 3D computed tomography (CT) baggage security imagery [32]–[34]. An extensive review is presented in [21], [22].

By contrast to the predominance of BoVW techniques [1], [2], [4], [6], [17], and the limited evaluation of recent developments from the CNN literature [7], [8] within this problem domain, we explicitly evaluate multiple CNN classification architectures [9], [14]–[16] across multiple contemporary detection (object localization) paradigms. Uniquely, we consider a side-by-side comparison of multiple CNN variants and detection paradigms against traditional BoVW for reference across varied and challenging X-ray security images datasets, which are highly representative of operational conditions.

### III. CLASSIFICATION

Automated threat screening task in X-ray baggage imagery can be considered as a classical image classification problem. Here we address this task using convolutional neural networks and transfer learning approaches based on the prior work of [9], [15], [16], [35]–[37], and expanding the earlier preliminary studies of [7], [8]. To these ends, we initially outline a brief generalized background for convolutional neural networks and transfer learning, and explain our approach to applying these techniques to object classification within X-ray baggage images.

#### A. Convolutional Neural Networks

Deep convolutional neural networks have been widely used in many challenging computer vision tasks such as image classification [16], object detection [11]–[13] and segmentation [38]

Krizhevsky *et al.* (AlexNet) [9] propose a network (i.e., similar to [39] but deeper and wider, having 5 *conv* layers with  $11 \times 11$  receptive filters and 3 *fc* layers, and 60 million parameters in total). This high-level of parametrization, and hence representational capacity, make the network susceptible to over-fitting in the traditional machine learning sense. The use of dropout, whereby hidden neurons are randomly

removed during the training process, is introduced to avoid over-fitting such that performance dependence on individual network elements is reduced in favor of cumulative error reduction and representational responsibility for the problem space. In addition to dropout which increases the robustness of the networks to over-fitting, ReLu [9] is another novel approach in this work introduced as an activation function for non-linearity. By following the success of this work, Zeiler and Fergus [40] design a similar architecture with smaller receptive fields (ZFNet). Furthermore, the work also introduces a new approach for the visualization of feature representations within networks [40].

Inspired by the favorable outcome of [9] and [40], network width is thoroughly explored in [14] via the comparison of three networks with varying width. By following this, Simonyan and Zisserman (VGG) [15] study the importance of network depth on classification accuracy by stacking convolutional layers with small  $3 \times 3$  receptive fields with a stride of 1. Not only does the use of small receptive filters increase non-linearity but also decrease the total number of parameters of the network. It is empirically shown that stack of  $3 \times 3$  convolutional filters within a network with varying depth between 11 to 19 layers can significantly improve the state-of-the-art.

He *et al.* (ResNet) [16] propose a simple yet powerful network by following the work in [41]. Input is first fed into two stacked *conv* layers, then is added to the output of the *conv* layers before non-linearity is applied. This approach is used up to 34 layers. For deeper networks such as 50, 101, 152, filter factorization is employed such that *conv* layers are stacked using  $1 \times 1$ ,  $3 \times 3$  and  $1 \times 1$  filters (bottleneck layer). The proposed approach significantly reduces the number of parameters needed for a deep network and outperforms the previous state-of-the-art.

#### B. Transfer Learning

Modern CNN architectures such as [9], [15], [16], [37] are trained on huge datasets such as ImageNet [42] which contains approximately a million of data samples and 1000 distinct class labels. However, the limited applicability of such training and parameter optimization techniques to problems where such

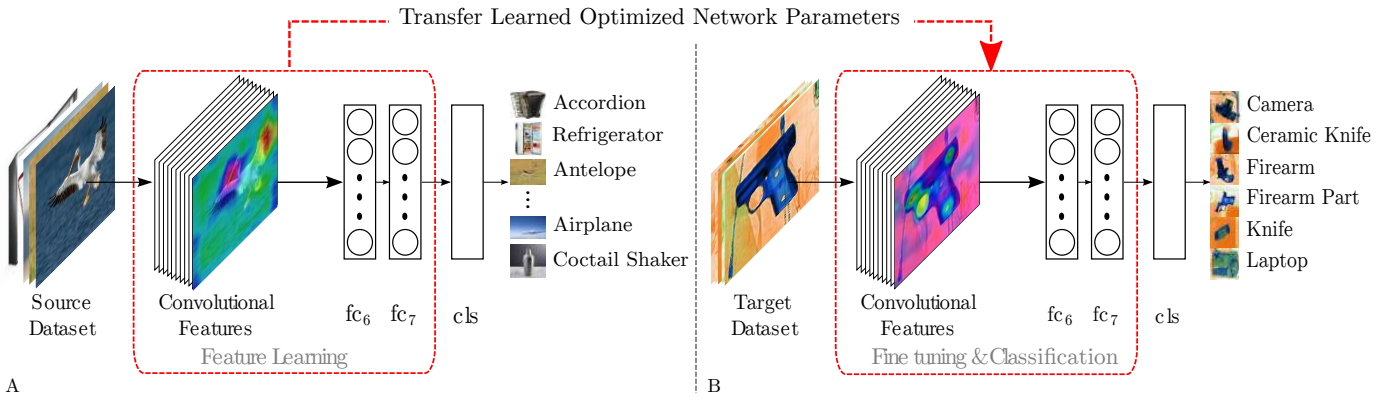


Fig. 3: Transfer learning pipeline. (A) shows classification pipeline for a source task, while (B) is a target task, initialized by the parameters learned in the source task.

large datasets are not available gives rise to the concept of transfer learning [35]. The work of [36] illustrated that each hidden layer in a CNN has distinct feature representation related characteristics among of which the lower layers provide general feature extraction capabilities (akin to Gabor filters and alike), while higher layers carry information that is increasingly more specific to the original classification task. Figure 2, for instance, demonstrates Gradient-based class activation map (Grad-CAM [30]) of VGG16 [15] for an example X-ray classification object. Lower layers - *i.e.*  $conv_{1-2}$  and  $conv_{2-2}$ , behave as edge detectors, while higher layers like  $conv_{4-3}$  and  $conv_{5-3}$  provides more specific representations belonging to the input image. This finding facilitates the verbatim re-use of the generalized feature extraction and representation of the lower layers in a CNN, while higher layers are fine-tuned towards secondary problem domains with related characteristics to the original. Using this paradigm, as demonstrated in Figure 3, we can leverage the *a priori* CNN parametrization of an existing fully trained network on a generic 1000+ object class problem [42] (Figure 3A), as a starting point for optimization towards to the specific problem domain of limited object class detection within X-ray images (Figure 3B). Instead of designing a new CNN with random weight initialization, we instead adopt a pre-trained CNN, pre-optimized for generalized object recognition, and fine-tune its weights towards our specific classification domain.

### C. Application to X-ray Security Imagery

To investigate the applicability of convolutional neural networks in object classification in X-ray baggage imagery, we address two specific target problems:- a) binary classification problem that performs firearm detection (*i.e.*, gun vs. no-gun) akin to that of the prior work of [4] to compare CNN features to conventional hand crafted attributes; b) a multi-class X-ray object classification problem (6 classes: firearm, firearm-components, knives, ceramic knives, camera and laptop), which further investigates the performance of CNN for the classification of multiple X-ray objects. The following subsection describes the datasets we use in our experiments.

1) *Datasets*: To perform classification tasks, we use four types of datasets described below:

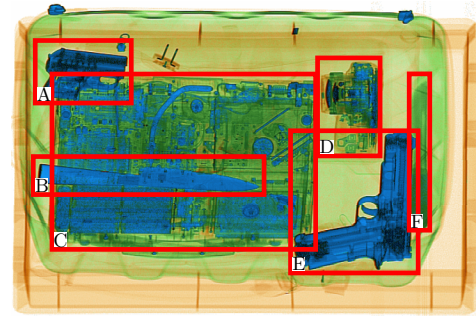


Fig. 4: Exemplar X-ray baggage image with extracted data set regions including background samples. Type of baggage objects in the dataset is as follows: (A) Firearm Component, (B) Ceramic Knife, (C) Laptop, (D) Camera, (E) Firearm, (F) Knife

**Dbp<sub>2</sub>**: Our data-set (11,627 X-ray images) are constructed using single conventional X-ray imagery with associated false color materials mapping from dual-energy [21]. To generate a dataset for firearm detection, we manually crop baggage objects, and label each accordingly (*e.g.*, Figure 4) - on the assumption an in-service detection solution would perform scanning window search through the whole baggage image. In addition to manual cropping, we also generate a set of negative images by randomly selecting  $256 \times 256$  fixed-sized overlapping image patches from a large corpus of baggage images that do not contain any target objects. Following these approaches, our evaluation datasets consist of 19,398 X-ray sample patches for a classical two-class firearms detection problem (positive class: 3,179 firearm images / 1,176 images of firearm components; negative class: 476 images of cameras, 2,750 knives, 1,561 ceramic knives, 995 laptops and 9,261 cropped images of background clutter)

**Dbp<sub>6</sub>**: For the multiple class problem, we separate firearms and firearm sub-components into two distinct classes to make the problem even more challenging. Likewise, regular and ceramic knives are considered as two different class objects, which overall we have a 6-class problem for the multi-class task (*i.e.*, each patch being either one of the six object labels).

In addition to these datasets, we also use UK government evaluation dataset [19], which is available upon request from UK Home Office Centre for Applied Science and Technology (CAST). This dataset comprises of both expertly concealed

firearm (threat) items and operational benign (non-threat) imagery from commercial X-ray security screening operations on the UK (baggage/parcels). From this dataset, we define two evaluation problems based on the provided annotation for the presence of firearms threat items.

**Full Firearm vs. Operational Benign - (FFOB):** comprising 4,680 firearm threat and 5,000 non-threat images, and is denoted as FFOB.

**Firearm Parts vs. Operational Benign - (FPOB):** contains 8,770 firearm and parts threat and 5,000 non-threat images (denoted FPOB, comprising of annotations as any of *{bolt carrier assembly, Pump action, Set, Shotgun, Sub-Machine-Gun}*).

We split the datasets into training (60%), validation (20%) and test sets (20%) such that each split has similar class distribution but unseen test set contains somewhat challenging samples never trained before. Besides, we also weight the data when sampling to cope with class imbalances. We also perform random flipping, random cropping, and rotation to each sample to augment the datasets.

2) *Classification:* Using transfer learning paradigm explained in Section III-B, this work leverages the *a priori* CNN parametrization of an existing fully trained network, on a generic 1000 object class problem [42], as a starting point for optimization towards another problem domain of limited object class detection within X-ray images.

For the binary classification problem, we specifically make use of the CNN configuration designed by Krizhevsky *et al.* [9], having 5 convolutional layers (*conv*), 3 fully-connected layers (*fc*), and trained on the ImageNet dataset on a 1000 class image classification problem, denoted as AlexNet [9].

The first step is to fine tune all of the *conv* and *fc* layers of the network via transfer learning on the training set of the target classification problem. In addition to this, we also perform layer freezing, meaning that instead of updating layer parameters for our task, we use the original unmodified weights from the initial trained CNN parametrization of [9]. This allows us to observe how fine-tuning each layer impacts the overall performance.

Also, having fine-tuned the parameters via this transfer learning approach, we extract the features of the last fully connected layer (*fc<sub>7</sub>*) to train on an SVM classifier. This allows us to additionally compare the internal feature space representation of the CNN model to alternative more traditional (handcrafted) BoVW features as used in prior work [4].

Evaluation of our proposed approach is performed against the prior SVM-driven work of Kundegorski *et al.* [4] within a BoVW framework. SVM are trained using Radial Basis Function (RBF) kernel  $\{SVM_{RBF}\}$  with a grid search over kernel parameter,  $\gamma = 2^x : x \in \{-15, 3\}$ , and model fitting cost,  $c = 2^x : x \in \{5, 15\}$ , using k-fold cross validation ( $k = 5$ ) with F-score optimization (being more representative than accuracy for unbalanced datasets). The results for the best performing parameter set are reported for each feature configuration.

The second set of experiments is the classification of multiple baggage objects, a more complex six class object problem. Here the lesser performing SVM with handcrafted

features are not considered (Table I), in favor of the CNN approach. Instead, we fine-tune AlexNet [9], VGG [15] and ResNet [16], each of which are top performing entries of ImageNet [42] competition. By doing so, we aim to evaluate the feasibility of CNN for this problem domain further.

To update the parameters of all the networks during training, we use cross-entropy for the loss function, and utilize Adam [44] optimizer with a learning rate of  $10^{-3}$ , and a weight decay of 0.005 since we observe that it achieves superior accuracy to SGD and RMS for this task. Our stopping criterion is to terminate optimization where validation starts to reduce, while training accuracy continues to improve. This fork between training and validation performance usually takes 30 epochs for this task.

#### D. Evaluation

The performance is evaluated by the comparison of True Positive Rate (TP) (%), False Positive Rate (FP) (%) together with Precision (P), Accuracy (A) and F-score (F) (harmonic mean of precision and true positive rate).

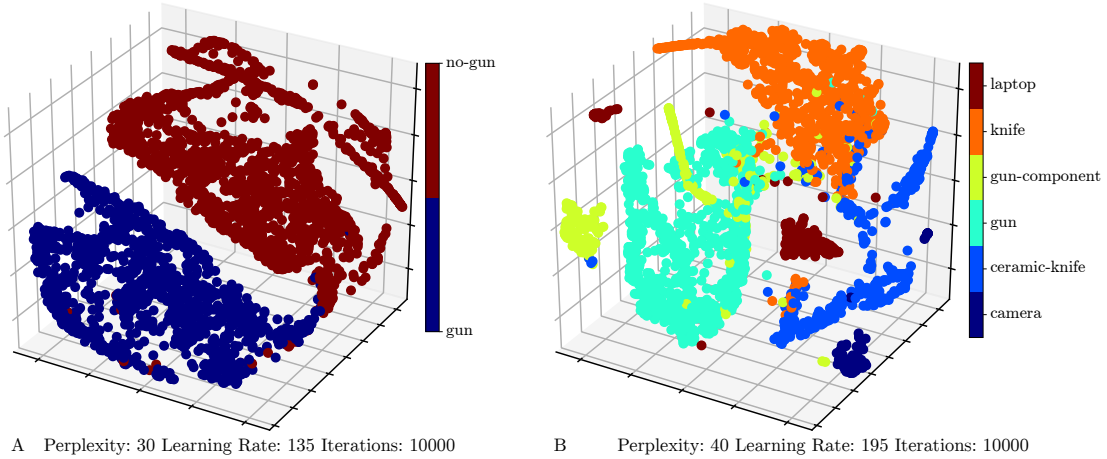
Results for the two class problem is given in Table I, which is divided into four sections: - first section lists the performance of the CNN approach, notated as  $AlexNet_{a,b}$ , meaning that the network is fine-tuned from layer *a* to layer *b*, while the rest of the layers are frozen (Table I, top). This means, for instance,  $AlexNet_{4-8}$  is trained by fine-tuning the layers  $\{4, 5, 6, 7, 8\}$  and freezing the layers  $\{1, 2, 3\}$  (i.e. remain unchanged from the pre-trained model of [9]). The second section has the results of an SVM classifier trained on the output of the last layer of CNN (Table I, middle upper). Similar to the first section, we again perform layer freezing here for a consistent comparison of CNN features and BoVW features. The third section shows fine tuning results based on contemporary end to end CNN architectures (VGG<sub>M</sub> [14], VGG<sub>16</sub> [15], ResNet<sub>18</sub> [16], ResNet<sub>50</sub> [16], ResNet<sub>101</sub> [16], Table I, middle lower). The last section lists the best performing BoVW feature detector/descriptor variants trained with SVM in the work of [4] (Table I, bottom).

Table I shows the performance results of firearm detection. We see that true and false positives have a general trend to decrease as the number of fine-tuned layers reduces. Likewise, freezing lower layers reduces the accuracy of the models.

Training an SVM classifier on CNN features with layer freezing yields relatively better performance than the standard end to end CNN results. Here, We see a performance pattern such that fine-tuning more layers has a positive impact on the overall performance. For instance, SVM trained on fully fine-tuned CNN has the highest performance on all of the metrics, outperforming the prior work of [4] and [7] (Table I).

For an end to end fine-tuning using contemporary architectures, we observe the direct proportion of performance and network complexity. ResNet<sub>101</sub> [16], for instance, is the best performing network among all of the end to end CNN networks (Table I).

It is also significant to note that the performance of the best feature detector/descriptor combination of BoVW approach (FAST/SURF [4]) is worse than any of the CNN features



A Perplexity: 30 Learning Rate: 135 Iterations: 10000

B Perplexity: 40 Learning Rate: 195 Iterations: 10000

Fig. 5: t-SNE [43] visualization of feature maps extracted from the last  $fc$  layer of VGG<sub>16</sub> [15] fine-tuned for binary (A) and multi-class (B) problems.

		TP%	FP%	P	A	F
A. CNN [9] Layer Freezing	AlexNet <sub>1-8</sub>	99.26	4.08	0.741	0.961	0.849
	AlexNet <sub>2-8</sub>	98.53	2.40	0.832	0.983	0.902
	AlexNet <sub>3-8</sub>	96.32	2.19	0.844	0.980	0.900
	AlexNet <sub>4-8</sub>	95.59	2.96	0.790	0.973	0.865
	AlexNet <sub>5-8</sub>	98.16	4.68	0.711	0.961	0.825
	AlexNet <sub>6-8</sub>	96.32	5.15	0.693	0.954	0.806
	AlexNet <sub>7-8</sub>	94.49	3.65	0.754	0.961	0.839
	AlexNet <sub>8</sub>	95.22	4.21	0.733	0.960	0.828
CNN [9] + SVM Layer Freezing	AlexNet <sub>1-8</sub>	<b>99.56</b>	<b>1.07</b>	<b>0.997</b>	<b>0.994</b>	<b>0.996</b>
	AlexNet <sub>2-8</sub>	99.30	1.50	0.996	0.991	0.994
	AlexNet <sub>3-8</sub>	99.18	1.93	0.995	0.989	0.993
	AlexNet <sub>4-8</sub>	98.92	1.86	0.995	0.988	0.992
	AlexNet <sub>5-8</sub>	98.80	2.07	0.994	0.986	0.991
	AlexNet <sub>6-8</sub>	98.68	3.00	0.991	0.983	0.983
	AlexNet <sub>7-8</sub>	98.64	4.15	0.989	0.980	0.980
	AlexNet <sub>8</sub>	98.42	5.43	0.985	0.976	0.976
CNN End to End	VGG <sub>M</sub> [14]	98.38	0.36	0.998	0.987	0.980
	VGG <sub>16</sub> [15]	99.08	1.14	0.997	0.990	0.985
	ResNet <sub>18</sub> [16]	99.38	1.43	0.996	0.992	0.988
	ResNet <sub>50</sub> [16]	99.54	1.00	0.998	0.995	0.992
	ResNet <sub>101</sub> [16]	99.66	1.14	0.997	0.995	0.993
BoVW SVM [4]	SURF/SURF	79.2	3.2	0.88	0.93	0.83
	KAZE/KAZE	77.3	3.9	0.85	0.92	0.81
	FAST/SURF	83.0	3.3	0.88	0.94	0.85
	FAST/SIFT	80.9	4.3	0.85	0.92	0.83
	SIFT/SIFT	68.3	4.2	0.83	0.90	0.75

TABLE I: Results of CNN and BoVW on Dbp<sub>2</sub> dataset for firearm detection. AlexNet<sub>ab</sub> denotes that the network is fine tuned from layer a to layer b.

given in Table I. Further comparison of BoVW+SVM against CNN+SVM proves the superiority of CNN features to traditional handcrafted features (Table I).

Table II shows the overall performance of the networks fine-tuned for multiple class problem. Like Table I, finetuning the entire network yields the best performance. A conclusion can be reached from these results that fine-tuning higher level layers and freezing lower ones have a detrimental impact on the performance of the CNN model. Similar to Table I, performance and network complexity are also directly proportional. With relatively lower complexity than the rest, AlexNet [9] has the lowest accuracy of 0.924. ResNet<sub>101</sub> [16], on the other hand, achieves the highest on all metrics (P=96.0% R=96.6%

	P	R	A	F
AlexNet <sub>1-8</sub>	0.911	0.904	0.904	0.906
AlexNet <sub>2-8</sub>	0.842	0.841	0.833	0.835
AlexNet <sub>3-8</sub>	0.843	0.841	0.844	0.841
AlexNet <sub>4-8</sub>	0.841	0.853	0.844	0.846
AlexNet <sub>5-8</sub>	0.833	0.821	0.823	0.811
AlexNet <sub>6-8</sub>	0.820	0.810	0.819	0.809
AlexNet <sub>7-8</sub>	0.774	0.793	0.722	0.761
AlexNet <sub>8</sub>	0.721	0.742	0.701	0.712
VGG <sub>M</sub> [14]	0.928	0.932	0.923	0.926
VGG <sub>16</sub> [15]	0.931	0.943	0.940	0.936
ResNet <sub>18</sub> [16]	0.933	0.943	0.936	0.937
ResNet <sub>50</sub> [16]	0.934	0.910	0.923	0.917
ResNet <sub>101</sub> [16]	<b>0.936</b>	<b>0.946</b>	<b>0.937</b>	<b>0.938</b>

TABLE II: Statistical evaluation of CNN architectures (AlexNet, VGG, and ResNet) on Dbp<sub>6</sub> dataset for multi-class problem.

	TP%	FP%	P	A	F
AlexNet [9]	99.830	0.943	0.990	0.994	0.994
VGG <sub>M</sub> [15]	99.010	0.000	1.000	0.995	0.995
VGG <sub>16</sub> [15]	99.831	0.000	1.000	0.999	0.999
ResNet <sub>18</sub> [16]	99.472	0.000	1.000	0.997	0.997
ResNet <sub>50</sub> [16]	100.00	0.923	0.990	0.995	0.995
ResNet <sub>101</sub> [16]	100.00	0.311	0.996	0.998	0.998

TABLE III: Statistical evaluation of varying CNN architectures (AlexNet, VGG, and ResNet) on FFOB dataset [19].

A=97.5% F=96.1%).

In addition, results are presented on the UK government evaluation dataset [19] in Tables III and IV. Within Table III and IV we present results for classification only (following the approach of Section III-B), where we can see comparable performance to the earlier results presented in Tables I and II.

	TP%	FP%	P	A	F
AlexNet [9]	95.088	3.527	0.960	0.958	0.958
VGG <sub>M</sub> [15]	95.864	0.919	0.990	0.974	0.974
VGG <sub>16</sub> [15]	97.238	4.217	0.954	0.965	0.964
ResNet <sub>18</sub> [16]	95.725	0.744	0.992	0.975	0.974
ResNet <sub>50</sub> [16]	99.411	1.060	0.988	0.991	0.991
ResNet <sub>101</sub> [16]	99.608	0.000	1.000	0.998	0.998

TABLE IV: Statistical evaluation of varying CNN architectures (AlexNet, VGG, and ResNet) on FFOB dataset [19].

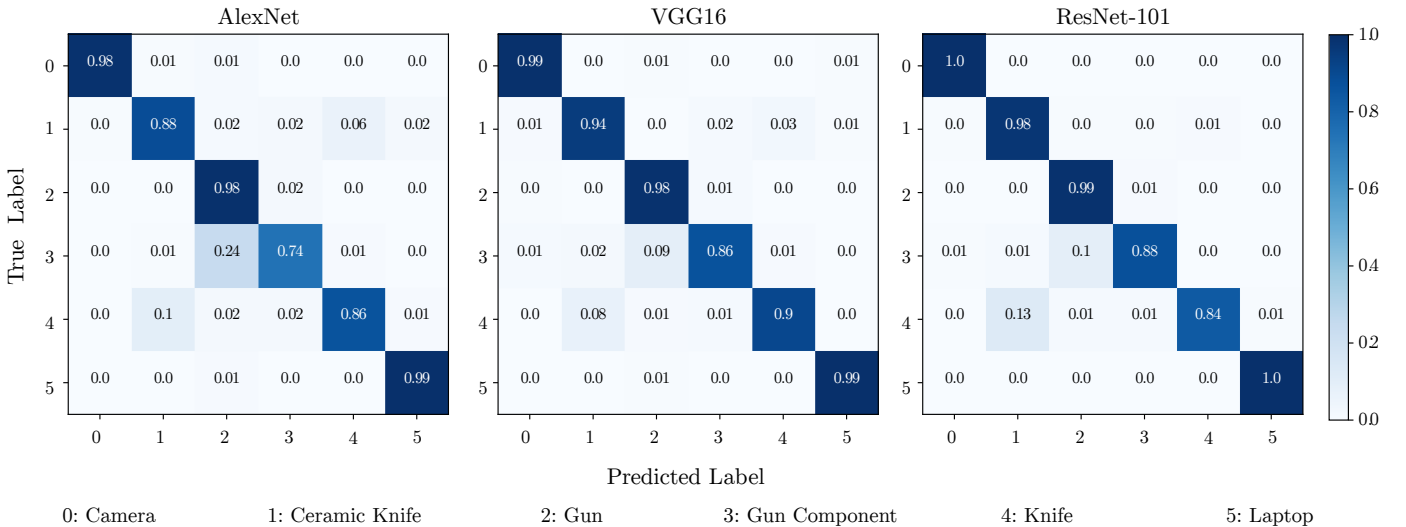


Fig. 6: Confusion matrices for AlexNet [9], VGG16 [15] ResNet-50 [16] fine tuned for multi class problem

Figure 5 depicts the t-SNE [43] visualization of feature maps of the down-projected internal feature space representation extracted from VGG<sub>16</sub> [15] fine-tuned for binary (A) and multi-class (B) problems. In both cases, classes are well separated, showing the capability of CNN features within this problem domain (Figure 5).

Figure 6 depicts per-class accuracy obtained via the use of AlexNet [9] and ResNet<sub>101</sub> [16], the worst and best performing networks within this task. We see that laptop and camera object classes are straightforward to classify. In contrast, networks have relatively lower classification confidence for knife, ceramic knife vs. firearm, firearm parts, which obviously stems from the similarity of the objects.

**Limitations:** Due to the cluttered nature of the input dataset, there are certain cases where CNN based classification fails to classify threats. Figure 7, for instance, demonstrates that CNN labels these image examples as laptops with high confidence, as the predominant object signature present in the image patch, while failing to detect the foreground objects of interest (yellow highlights, Figure 7). This results in a significant increase in false negative occurrences (Table II). We consider this primarily as an object detection problem, and hence explore the contemporary object detection strategies in the subsequent part of this study.

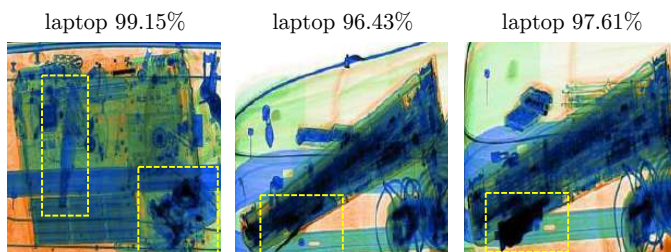


Fig. 7: Exemplar image cases where CNN (only) classification fails to detect an object in the presence of clutter and other confusing items of interest (here: background laptop detected, knives/guns missed).

#### IV. OBJECT DETECTION

From Section III, the approach of CNN based classification via transfer learning yields promising performance especially for single and non-occluded X-ray image patches. When it comes to classifying multiple objects (Figure 7), however, more sophisticated approaches are needed to perform joint localization. Here we give a brief introduction to CNN based object detection algorithms for an exhaustive evaluation within X-ray baggage domain.

##### A. Background

Sermanet *et al.* (OverFeat) [18] uses a sliding window approach to generate the region proposals, which is then fed into a convolutional neural network for the classification. The key idea here is that bounding box regression is performed with an extra regression layer which shares the weights with the main network. Subsequent work [45] proposes a detection algorithm (RCNN), based on three main stages: region proposal generation, feature extraction, and classification. The first stage employs an external region proposal generator, followed by a fine-tuned CNN in the next stage for feature extraction. The final stage performs classification with an SVM classifier. Even though it outperforms previous work by a large margin, this model is not considered to be real-time applicable due to runtime and memory issues. In contrast, SPPNet [46] contains variable-sized spatial pooling layer between the convolutional and fully connected layers, which allows the network to handle images of arbitrary scales and aspect ratios. With this design, image representations can be computed once in SPPNet, which makes the network significantly faster than RCNN. Like RCNN, however, the network has several separate stages, which is computationally expensive. Fast RCNN by Girshick [47] combines feature extraction, classification and bounding box regression stages by designing a partially end to end CNN network, significantly outperforming [45], [46] regarding speed and accuracy. The novelty of the work is to employ a region of interest pooling layer (RoI) before fully connected layers ( $fc$ ) to fix the size of the region

proposals generated by the region proposal algorithm. These fixed sized object localization proposals are then classified via  $fc$  layers. In addition to the classification, bounding box regression is also performed via a multi-task loss function to localize objects of interests with a bounding rectangle. The limitation, however, is that the network still needs an external region proposal algorithm such as selective search [48]. Inspired by the strong and weak points of [45]–[47], Ren *et al.* [11] propose a model, named Faster RCNN (F-RCNN) performing all the aforementioned stages in an end to end deep neural network. This approach not only reduces time complexity and required memory but also significantly boosts overall performance. Further optimization of this concept by [12] proposes a fully convolutional detection framework (R-FCN), which yields faster training and testing performance with competitive accuracy compared to F-RCNN [11].

In this work, we adapt F-RCNN, R-FCN and YOLOv2 each of which provide a significant boost in accuracy, for use within an X-ray baggage object detection context, and compare with previous object detection approaches primarily based on traditional sliding window detection frameworks [5], [10].

### B. Detection Strategies

Within this work, we consider a number of competing contemporary detection frameworks and explore their applicability and performance for generalized object detection in X-ray baggage imagery.

**Sliding Window Based CNN** detection consists of two main stages, one of which is to generate objects of interests, while the other one performs classification. To create objects of interest, a fixed sized  $n \times n$  window slides over the image horizontally and vertically denoting the current region of interest. The disadvantage of using fixed sized window is that large objects may not fit within the window, resulting in weaker proposal generation. The use of image pyramids addresses this issue via the use of multi-scale sampling of the image and subsequent image interpolation of window regions at differing scale to a fixed size classification region input size. First two stages of Figure 8A demonstrate region proposal generation process for a sliding window approach. After generating this region of interest proposals, each is evaluated by the second stage of classification (here using a CNN as per Section III, Figure 8A). As described in Section III, with the use of transfer learning approach, CNN extracts convolutional features and performs classification via fully-connected layers. This method is similar to an external region proposal generator (sliding window traversal of the image) followed by CNN classification.

**Faster RCNN (F-RCNN)** is based on two subnetworks, containing a unique region proposal network (RPN) and Fast RCNN network together [11]. Instead of utilizing an external region proposal algorithm as in [45], [47], this model has its region proposal network (the main differentiator from Fast RCNN [47]). The RPN consists of convolutional layers that generate set of anchors with different scales and aspect ratios, and predict their bounding box coordinates together with a probability score denoting whether the region is an object or

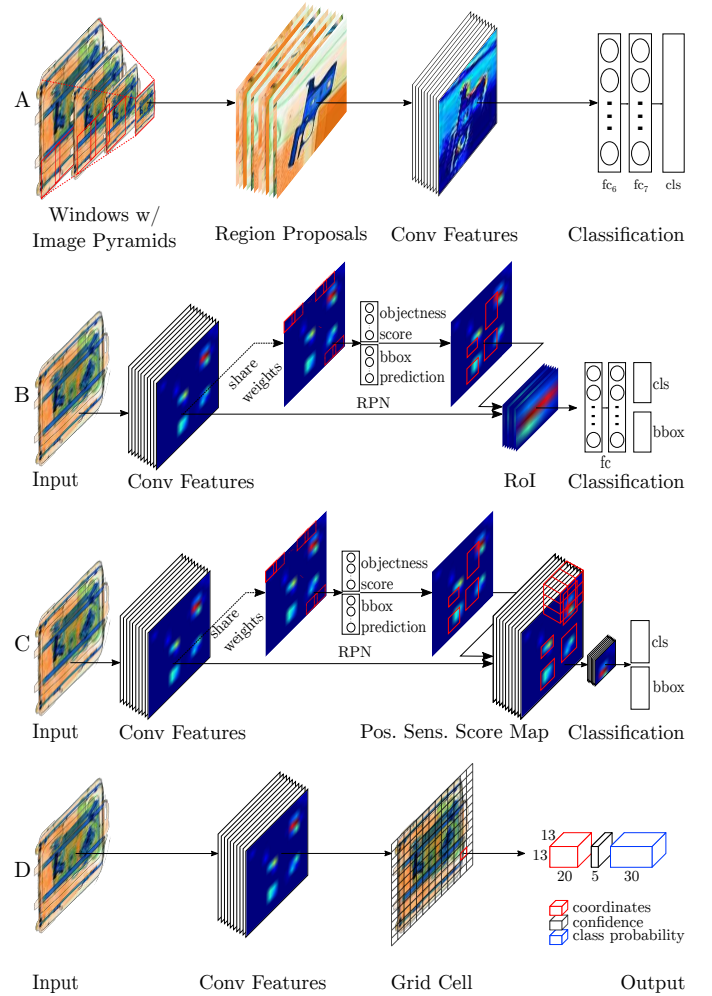


Fig. 8: Schematics for the CNN driven detection strategies evaluated. A. Sliding Window based CNN (SW-CNN) [4], [7], B. Faster RCNN (F-RCNN) [11], C. R-FCN [12], D. YOLOv2 [13]).

background. Anchors are generated by spatially sliding a  $3 \times 3$  window through the feature maps of the last convolutional layers of the Fast RCNN network. These features are then fed to objectness classification and bounding box regression layers. Objectness classification layer classifies whether a region proposal is an object or a background while bounding box regression layer predicts the coordinates of the area. An RoI pooling layer resizes these regions to fixed sized dimensions.  $fc$  layers then create feature vectors to be used by bounding box regression and softmax layers (see Figure 8B).

**R-FCN**, proposed by Dai *et al.* [12], points out the main limitation of Faster RCNN in that each region proposal within RoI pooling layer is computed numerous of times due to the two subsequent fully connected layers, which is computationally expensive (Figure 8B). They propose a new approach by removing fully-connected layers after RoI pooling, and employing a new variant denoted as “*position sensitive score map*” [12], which handles translation variance issue in detection task (Figure 8C). Removing fully connected subnetworks leads to much faster convergence both in training and test stages, while achieving similar detection performance results to Faster RCNN [11].

**YOLOv2** [13] is a fully CNN that achieves state-of-the-art results for object detection. It uses specific techniques to improve its performance against the prior work. Its initial novelty stems from the fact that it performs detection in a single forward-pass, while region-based approaches utilize sub-network for region generation. Like Faster RCNN, it also employs anchors. The main difference here, however, is that instead of fixing the anchor parameters, this approach makes use of  $k$ -means clustering over the input data to learn the anchor parameters of the ground truth bounding boxes. In addition to anchors, YOLOv2 performs batch normalization after each layer, resulting in an improvement in the overall performance. Another strategy is the use of higher resolution input images together with multi-scale training. Unlike classification networks that inputs smaller size images such as  $224 \times 224$ , YOLOv2 accepts inputs with higher resolution varying between  $350 \times 350$  to  $600 \times 600$ . Besides, the model randomly resizes input images during the training, which allows the network to work with objects with varying scales, and hence handles scaling issue. The above strategies yield significant performance improvements, and the approach achieves the state-of-the-art.

The way YOLOv2 works is rather novel. It divides the input into  $13 \times 13$  grid cells, each of which predicts 5 bounding box coordinates for each anchor. Moreover, for individual predicted bounding boxes, the network outputs confidence score showing the similarity between the bounding boxes and the ground truth. Finally, the output also includes the probability distribution of the classes that the predicted bounding boxes belong. Performing regression and classification within a single network makes YOLOv2 significantly faster, achieving real-time performance.

#### C. Application to X-ray Security Imagery

We compare four localization strategies for our object detection task within X-ray security imagery: a traditional sliding window approach [10] coupled with CNN classification [18], Faster RCNN (F-RCNN) approach of [11] (a contemporary architecture within recent object recognition challenge results [42], [49]), R-FCN approach of [12] (comparable to F-RCNN in performance yet offering significant computational efficiency gains over the former), and YOLOv2 [13], which currently achieves the best detection performance on PASCAL VOC benchmark while keeping the computation in real-time. **Dataset:** Instead of using multi-view conventional X-ray patches that we manually crop for the classification task in Section III, here we use full X-ray images to perform binary and multiple class object detection.

**Detection:** For sliding window CNN (SW-CNN) we employ  $800 \times 800$  input image,  $50 \times 50$  fixed size window with a step size of 32 to generate region proposals. We also use image pyramids to fit the window to varying sized objects using 9 pyramid levels. For the classification of the proposed regions we use AlexNet [9], VGG<sub>M,16</sub> [15], and ResNet-{50, 101} [16] networks. Although [18] employs an extra bounding box regression layer within their SW-CNN approach, we do not perform regression as none of the prior work within this domain does so [5], [10].

For Faster RCNN [11] we use the original implementation with a few modifications, and train Faster RCNN with AlexNet [9], VGG<sub>M,16</sub> [15], and ResNet-{50, 101} [16] architectures. Since R-FCN is fully convolutional by design, we only use ResNet-{50, 101} [16] networks for R-FCN to train and test.

For the training of the detection strategies explained here, we employ transfer learning approach and use the networks pre-trained on ImageNet dataset [42]. In so doing not only increases performance but also reduces training time significantly. We use stochastic gradient descent (SGD) with momentum and weight decay of 0.9 and 0.0005, respectively. The initial learning rate of 0.001 is divided by 10 with step down method in every 10,000 iteration. For F-RCNN/R-FCN, batch size is set to 256 for the RPN. All of the networks are trained by using dual-core Intel Xeon E5-2630 v4 processor and Nvidia GeForce GTX Titan X GPU.

#### D. Evaluation

Performance of the models is evaluated by mean average precision (mAP), used for PASCAL VOC object detection challenge [50]. To calculate mAP, we perform the following: we first sort  $n_d$  detections based on their confidence scores. Next, we calculate the area of intersection over union for the given ground truth and detected bounding boxes for each detection as

$$\Psi(B_{gt_i}, B_{dt_i}) = \frac{\text{Area}(B_{gt_i} \cap B_{dt_i})}{\text{Area}(B_{gt_i} \cup B_{dt_i})}, \quad (1)$$

where  $B_{gt_i}$  and  $B_{dt_i}$  are ground truth and detected bounding boxes for detection  $i$ , respectively. Assuming each detection as unique, and denoting the area as  $a_i$ , we then threshold it by  $\theta = 0.5$  giving a logical  $b_i$ , where

$$b_i = \begin{cases} 1 & a_i > \theta; \\ 0 & \text{otherwise.} \end{cases} \quad (2)$$

This is followed by a prefix-sum giving both true positives  $\vec{t}$  and false positives  $\vec{f}$ , where

$$\begin{aligned} t_i &= t_{i-1} + b_i, \\ f_i &= t_{i-1} + (1 - b_i). \end{aligned} \quad (3)$$

The precision  $\vec{p}$  and recall  $\vec{r}$  curves are calculated as

$$\begin{aligned} p_i &= \frac{t_i}{t_i + f_i}, \\ r_i &= \frac{t_i}{n_p}, \end{aligned} \quad (4)$$

where  $n_p$  is the number of positive samples. For a smoother curve, precision vector is then interpolated by using

$$p_i = \max(p_i, p_{i+1}). \quad (5)$$

We then calculate average precision (AP) based on the area under precision ( $\vec{p}$ ) recall ( $\vec{r}$ ) curve

$$AP = \sum_i^{n_d} p_i \Delta r. \quad (6)$$

Model	Network	mAP	camera	laptop	gun	gun component	knife	ceramic knife
SWCNN	AlexNet	0.608	0.682	0.609	0.748	0.714	0.212	0.683
	VGG <sub>M</sub>	0.634	0.707	0.637	0.763	0.731	0.246	0.719
	VGG <sub>16</sub>	0.649	0.701	0.724	0.752	0.757	0.223	0.734
	ResNet <sub>50</sub>	0.671	0.692	0.801	0.747	0.761	0.314	0.713
	ResNet <sub>101</sub>	0.776	0.881	0.902	0.831	0.848	0.392	0.803
RCNN	AlexNet	0.647	0.791	0.815	0.853	0.582	0.188	0.658
	VGG <sub>M</sub>	0.686	0.799	0.855	0.869	0.658	0.210	0.723
	VGG <sub>16</sub>	0.779	0.888	<b>0.954</b>	0.876	0.832	0.304	0.819
F-RCNN	AlexNet	0.788	0.893	0.756	0.914	0.874	0.467	0.823
	VGG <sub>M</sub>	0.823	<b>0.900</b>	0.834	0.918	0.875	0.542	0.869
	VGG <sub>16</sub>	0.883	0.881	0.918	0.927	<b>0.938</b>	0.721	0.912
	ResNet <sub>50</sub>	0.851	0.844	0.879	0.916	0.901	0.677	0.889
	ResNet <sub>101</sub>	0.874	0.857	0.904	0.931	0.911	<b>0.732</b>	0.907
R-FCN	ResNet <sub>50</sub>	0.846	0.894	0.928	0.932	0.918	0.506	0.896
	ResNet <sub>101</sub>	0.856	0.887	0.906	0.942	0.925	0.556	<b>0.920</b>
YOLOv2	Darknet <sub>288</sub>	0.810	0.821	0.861	0.914	0.904	0.551	0.814
	Darknet <sub>416</sub>	0.851	0.888	0.883	<b>0.952</b>	0.924	0.605	0.851
	Darknet <sub>544</sub>	<b>0.885</b>	0.896	0.894	0.943	0.933	0.728	0.913

TABLE V: Detection results of SW-CNN, Fast-RCNN (F-RCNN) [47], Faster RCNN (F-RCNN) [11], R-FCN [12] and YOLOv2 [13] for multi-class problem (300 region proposals). Class names indicates corresponding average precision (AP) of each class, and mAP indicates mean average precision of the classes.

As shown in Eq 7, we finally find mAP by averaging AP values that we calculate for  $C$  classes.

$$mAP = \frac{1}{C} \sum_{c=1}^C AP_c \quad (7)$$

Tables V and VI show binary and multi-class detection results for SW-CNN, F-RCNN, R-FCN with varying networks, and a fixed sized number of region proposals of 300, and for YOLOv2 with a fixed network with varying input image size. For completeness, we additionally present the comparative results for Fast R-CNN (RCNN) [47] (detection architecture pre-dating that of F-RCNN [11] and R-FCN [11]).

As a general trend, we observe that performance increases with overall network complexity such that superior performance is obtained with VGG16 and ResNet<sub>101</sub> for the region-based approaches. This observation holds for both the 2-class and 6-class problems considered here. Overall, YOLOv2 yields the leading performance for both 2-class and 6-class problems. In addition to this set of experiments, we also train the detection approaches using the pre-trained weights of Dbp6 dataset introduced in Section III-C1. Since not observing significant nuances in results, we do not include them here.

For the multi-class detection task (Table V) we see a similar performance pattern to that seen in the earlier firearm detection task. Here, SW-CNN performs worse than any network trained using a Faster RCNN or R-FCN architecture. Similarly, overall mAP of RCNN is lower than any R-FCN and R-FCN architecture. For comparison of F-RCNN and R-FCN, we observe that Faster RCNN achieves its highest peak using VGG16, with higher mAP than ResNet-50 and ResNet101. R-FCN with ResNet-50 and ResNet<sub>101</sub> yields slightly worse performance, (mAP: 0.846, 0.856), than that of the best of Faster-RCNN. For the overall performance comparison, YOLOv2 with an input size of 544×544 shows superior performance (mAP: 0.885).

For firearm detection Table VI shows that SW-CNN, even with a complex second stage classification CNN such as VGG16 and ResNet<sub>101</sub>, performs poorly compared to any other detection approaches. This poor performance is primarily due to lacking a bounding box regression layer (Figure 8), a significant performance booster as shown in [18], [45]. Likewise, the best performance of RCNN with VGG16 (mAP: 0.854) is worse than any F-RCNN or R-FCN. This is because the RPN within F-RCNN and R-FCN provides superior object proposals than the selective-search approach used in RCNN. For overall performance on the binary firearm detection task, R-FCN with YOLOv2 with an input image of size 416×416 yields the highest mAP of 0.974.

Model	Network	mAP - firearm
SW-CNN	AlexNet	0.753
	VGG <sub>M</sub>	0.772
	VGG <sub>16</sub>	0.806
	ResNet <sub>50</sub>	0.836
	ResNet <sub>101</sub>	0.847
RCNN	AlexNet	0.823
	VGG <sub>M</sub>	0.836
	VGG <sub>16</sub>	0.854
F-RCNN	AlexNet	0.945
	VGG <sub>M</sub>	0.948
	VGG <sub>16</sub>	0.960
	ResNet <sub>50</sub>	0.951
	ResNet <sub>101</sub>	0.960
R-FCN	ResNet <sub>50</sub>	0.949
	ResNet <sub>101</sub>	0.963
YOLOv2	Darknet <sub>288</sub>	0.931
	Darknet <sub>416</sub>	<b>0.974</b>
	Darknet <sub>544</sub>	0.962

TABLE VI: Detection results of SW-CNN, Fast-RCNN (RCNN) [47], Faster RCNN (F-RCNN) [11], R-FCN [12] and YOLOv2 [13] for firearm detection problem (300 region proposals).

Figure 9 illustrates the impact on the number of region

proposals and input image sizes on both detection performance and runtime. Figure 9A-B demonstrate detection performance of the approaches on 2-class and 6-class detection tasks, respectively. Increase in the number of region proposals and input image size lead to a rise in detection performance. Overall, YOLOv2 achieves the highest detection on both tasks. Figure 9C shows mean runtime in frame per second (fps) where we can see YOLOv2 significantly outperforms the rest of the detection approaches. The lowest fps YOLOv2 achieves (50fps) is still considerably better than the best runtime R-FCN (20), F-RCNN (2.9) and SW-CNN (0.8) achieve.

Figure 10 illustrates qualitative examples extracted from the statistical performance analysis of Table V. We see that detection approaches can cope with cluttered datasets where classification methods can fail as shown in Figure 7.

## V. CONCLUSION

In this work, we exhaustively explore the use of CNN in the tasks of classification and detection within X-ray baggage imagery. For the classification problem, we make a comparison between CNN and traditional BoVW approaches based on handcrafted features. To do so, we perform layer freezing to observe the relative performance of fixed and fine-tuned sets of CNN feature maps. In addition to this, we train SVM classifier on top of the last layer of the network to have a consistent comparison between CNN and handcrafted features. We also explore various CNN to see the impact of network complexity on overall performance.

Experimentation demonstrates that CNN features achieve superior performance to handcrafted BoVW features. Fine tuning the entire network for this problem yields 0.996% True Positive (TP), 0.011 False Positive (FP) and 0.994 accuracy (A), a significant improvement on the best performing handcrafted feature detector/descriptor (FAST/SURF, 0.830 TP, 0.033 FP, 0.940 A). For the classification of multiple X-ray baggage objects, ResNet-50 achieves 0.986 (A), clearly demonstrating the applicability of CNN within X-ray baggage imagery, and outperforming prior reported results in the field [1]–[5].

In addition to classification, we also study object detection strategies to improve the performance of cluttered datasets further, where classification techniques fail. Hence, we examine the relative performance of traditional sliding window driven detection with CNN model [10], [18] against contemporary region-based [11], [12], [47] and single forward-pass based [13] CNN variants. We show that contemporary Faster RCNN, R-FCN, and YOLOv2 approaches outperform SW-CNN, which is already empirically shown to outperform handcrafted features, regarding both speed and accuracy. YOLOv2 yields 0.885 and 0.974 mAP over 6-class object detection and 2-class firearm detection problems, respectively. This result illustrates the real-time applicability and superiority of such integrated region based detection models within this X-ray security imagery context.

Future work will consider exploiting multi-view X-ray security imagery in an end to end design.

## ACKNOWLEDGMENT

The authors would like to thank the UK Home Office for partially funding this work. Views contained within this paper are not necessarily those of the UK Home Office.

## REFERENCES

- [1] M. Baştan, M. R. Yousefi, and T. M. Breuel, **Visual Words on Baggage X-Ray Images**. Berlin, Heidelberg: Springer Berlin Heidelberg, 2011, pp. 360–368. [Online]. Available: [http://dx.doi.org/10.1007/978-3-642-23672-3\\_44](http://dx.doi.org/10.1007/978-3-642-23672-3_44) 1, 2, 3, 11
- [2] D. Turcsany, A. Mouton, and T. P. Breckon, “Improving feature-based object recognition for x-ray baggage security screening using primed visualwords,” in **2013 IEEE International Conference on Industrial Technology**, Feb 2013, pp. 1140–1145. 1, 2, 3, 11
- [3] M. Bastan, W. Byeon, and T. M. Breuel, “Object recognition in multi-view dual energy x-ray images,” in **BMVC**, 2013. 1, 2, 11
- [4] M. Kundegorski, S. Akçay, M. Devereux, A. Mouton, and T. P. Breckon, “On using feature descriptors as visual words for object detection within x-ray baggage security screening,” in **International Conference on Imaging for Crime Detection and Prevention, IET (November 2016)**. 1, 2, 3, 4, 5, 6, 8, 11
- [5] M. Baştan, “Multi-view object detection in dual-energy x-ray images,” **Machine Vision and Applications**, vol. 26, no. 7-8, pp. 1045–1060, 2015. 1, 2, 8, 9, 11
- [6] D. Mery, E. Svec, and M. Arias, **Object Recognition in Baggage Inspection Using Adaptive Sparse Representations of X-ray Images**. Cham: Springer International Publishing, 2016, pp. 709–720. [Online]. Available: [http://dx.doi.org/10.1007/978-3-319-29451-3\\_56](http://dx.doi.org/10.1007/978-3-319-29451-3_56) 1, 2, 3
- [7] S. Akçay, M. E. Kundegorski, M. Devereux, and T. P. Breckon, “Transfer learning using convolutional neural networks for object classification within x-ray baggage security imagery,” in **Image Processing (ICIP), 2016 IEEE International Conference on**. IEEE, 2016, pp. 1057–1061. 1, 2, 3, 5, 8
- [8] D. Mery, E. Svec, M. Arias, V. Rizzo, J. M. Saavedra, and S. Banerjee, “Modern computer vision techniques for x-ray testing in baggage inspection,” **IEEE Transactions on Systems, Man, and Cybernetics: Systems**, vol. 47, no. 4, pp. 682–692, 2017. 1, 2, 3
- [9] A. Krizhevsky, I. Sutskever, and G. E. Hinton, “Imagenet classification with deep convolutional neural networks,” in **Advances in neural information processing systems**, 2012, pp. 1097–1105. 1, 2, 3, 5, 6, 7, 9
- [10] T. Franzel, U. Schmidt, and S. Roth, **Object detection in multi-view X-ray images**. Springer, 2012, pp. 144–154. 1, 2, 8, 9, 11
- [11] S. Ren, K. He, R. Girshick, and J. Sun, “Faster r-cnn: Towards real-time object detection with region proposal networks,” in **Advances in neural information processing systems**, 2015, pp. 91–99. 1, 2, 3, 8, 9, 10, 11
- [12] J. Dai, Y. Li, K. He, and J. Sun, “R-FCN: object detection via region-based fully convolutional networks,” **CoRR**, vol. abs/1605.06409, 2016. [Online]. Available: <http://arxiv.org/abs/1605.06409> 1, 2, 3, 8, 9, 10, 11
- [13] J. Redmon and A. Farhadi, “YOLO9000: Better, Faster, Stronger,” **ArXiv e-prints**, Dec. 2016. 1, 3, 8, 9, 10, 11
- [14] K. Chatfield, K. Simonyan, A. Vedaldi, and A. Zisserman, “Return of the devil in the details: Delving deep into convolutional nets,” **CoRR**, vol. abs/1405.3531, 2014. [Online]. Available: <http://arxiv.org/abs/1405.3531> 2, 3, 5, 6
- [15] K. Simonyan and A. Zisserman, “Very deep convolutional networks for large-scale image recognition,” **CoRR**, vol. abs/1409.1556, 2014. [Online]. Available: <http://arxiv.org/abs/1409.1556> 2, 3, 4, 5, 6, 7, 9
- [16] K. He, X. Zhang, S. Ren, and J. Sun, “Deep residual learning for image recognition,” in **Proceedings of the IEEE Conference on Computer Vision and Pattern Recognition**, 2016, pp. 770–778. 2, 3, 5, 6, 7, 9
- [17] D. Mery, V. Rizzo, I. Zuccar, and C. Pieringer, “Object recognition in x-ray testing using an efficient search algorithm in multiple views,” **Insight-Non-Destructive Testing and Condition Monitoring**, vol. 59, no. 2, pp. 85–92, 2017. 2, 3
- [18] P. Sermanet, D. Eigen, X. Zhang, M. Mathieu, R. Fergus, and Y. LeCun, “Overfeat: Integrated recognition, localization and detection using convolutional networks,” **CoRR**, vol. abs/1312.6229, 2013. [Online]. Available: <http://arxiv.org/abs/1312.6229> 2, 7, 9, 10, 11
- [19] “OSCT Borders X-ray Image Library, UK Home Office Centre for Applied Science and Technology (CAST),” Publication Number: 146/16, 2016. [Online]. Available: <https://www.gov.uk/government/collections/centre-for-applied-science-and-technology-information> 2, 4, 6

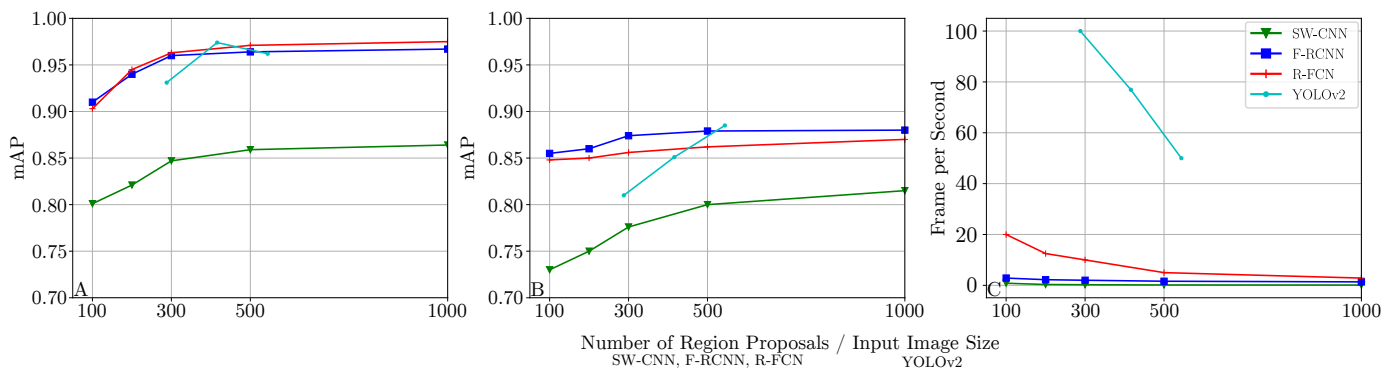


Fig. 9: Impact of number of box proposals on performance. (A) for binary class (B) for multi-class (C) Runtime. Models are trained using ResNet<sub>101</sub>

- [20] S. Singh and M. Singh, “Explosives detection systems (eds) for aviation security,” *Signal Processing*, vol. 83, no. 1, pp. 31–55, 2003. 2
- [21] A. Mouton and T. P. Breckon, “A review of automated image understanding within 3D baggage computed tomography security screening,” *Journal of X-ray science and technology*, vol. 23, no. 5, pp. 531–555, 2015. 2, 3, 4
- [22] T. W. Rogers, N. Jaccard, E. J. Morton, and L. D. Griffin, “Automated x-ray image analysis for cargo security: Critical review and future promise,” *Journal of X-ray science and technology*, vol. 25, no. 1, pp. 33–56, 2017. 2, 3
- [23] Z. Chen, Y. Zheng, B. R. Abidi, D. L. Page, and M. A. Abidi, “A combinational approach to the fusion, de-noising and enhancement of dual-energy x-ray luggage images,” in *Computer Vision and Pattern Recognition-Workshops, 2005. IEEE Computer Society Conference On*. IEEE, 2005, pp. 2–2. 2
- [24] B. R. Abidi, Y. Zheng, A. V. Gribok, and M. A. Abidi, “Improving weapon detection in single energy x-ray images through pseudocoloring,” *IEEE Transactions on Systems, Man, and Cybernetics, Part C (Applications and Reviews)*, vol. 36, no. 6, pp. 784–796, 2006. 2
- [25] Q. Lu and R. W. Conners, “Using image processing methods to improve the explosive detection accuracy,” *IEEE Transactions on Systems, Man, and Cybernetics, Part C (Applications and Reviews)*, vol. 36, no. 6, pp. 750–760, 2006. 2
- [26] M. Singh and S. Singh, “Image segmentation optimisation for x-ray images of airline luggage,” in *Computational Intelligence for Homeland Security and Personal Safety, 2004. Proceedings of the 2004 IEEE International Conference on*. IEEE, 2004, pp. 10–17. 2
- [27] G. Heitz and G. Chechik, “Object separation in x-ray image sets,” in *Computer Vision and Pattern Recognition, 2010 IEEE Conference on*. IEEE, 2010, pp. 2093–2100. 2
- [28] D. Mery, “Automated detection in complex objects using a tracking algorithm in multiple x-ray views,” in *Computer Vision and Pattern Recognition Workshops, 2011 IEEE Computer Society Conference on*. IEEE, 2011, pp. 41–48. 2
- [29] L. Schmidt-Hackenberg, M. R. Yousefi, and T. M. Breuel, “Visual cortex inspired features for object detection in x-ray images,” in *Pattern Recognition, 2012 21st International Conference on*. IEEE, 2012, pp. 2573–2576. 2
- [30] R. R. Selvaraju, A. Das, R. Vedantam, M. Cogswell, D. Parikh, and D. Batra, “Grad-cam: Why did you say that? visual explanations from deep networks via gradient-based localization,” *CoRR*, vol. abs/1610.02391, 2016. [Online]. Available: <http://arxiv.org/abs/1610.02391> 3, 4
- [31] N. Dalal and B. Triggs, “Histograms of oriented gradients for human detection,” in *Computer Vision and Pattern Recognition, 2005. CVPR 2005. IEEE Computer Society Conference on*, vol. 1. IEEE, 2005, pp. 886–893. 2
- [32] G. Flitton, T. P. Breckon, and N. Megherbi, “A comparison of 3D interest point descriptors with application to airport baggage object detection in complex CT imagery,” *Pattern Recognition*, vol. 46, no. 9, pp. 2420–2436, 2013. 3
- [33] G. Flitton, A. Mouton, and T. P. Breckon, “Object classification in 3D baggage security computed tomography imagery using visual codebooks,” *Pattern Recognition*, vol. 48, no. 8, pp. 2489–2499, 2015. 3
- [34] A. Mouton and T. P. Breckon, “Materials-based 3D segmentation of unknown objects from dual-energy computed tomography imagery in baggage security screening,” *Pattern Recognition*, vol. 48, no. 6, pp. 1961–1978, 2015. 3
- [35] M. Oquab, L. Bottou, I. Laptev, and J. Sivic, “Learning and transferring mid-level image representations using convolutional neural networks,” in *Proceedings of the IEEE conference on computer vision and pattern recognition*, 2014, pp. 1717–1724. 3, 4
- [36] J. Yosinski, J. Clune, Y. Bengio, and H. Lipson, “How transferable are features in deep neural networks?” in *Advances in neural information processing systems*, 2014, pp. 3320–3328. 3, 4
- [37] C. Szegedy, W. Liu, Y. Jia, P. Sermanet, S. Reed, D. Anguelov, D. Erhan, V. Vanhoucke, and A. Rabinovich, “Going deeper with convolutions,” *CoRR*, vol. abs/1409.4842, 2014. [Online]. Available: <http://arxiv.org/abs/1409.4842> 3
- [38] V. Badrinarayanan, A. Kendall, and R. Cipolla, “Segnet: A deep convolutional encoder-decoder architecture for image segmentation,” *CoRR*, vol. abs/1511.00561, 2015. [Online]. Available: <http://arxiv.org/abs/1511.00561> 3
- [39] Y. Lecun, L. Bottou, Y. Bengio, and P. Haffner, “Gradient-based learning applied to document recognition,” *Proc of the IEEE*, vol. 86, no. 11, pp. 2278–2324, Nov 1998. 3
- [40] M. D. Zeiler and R. Fergus, “Visualizing and understanding convolutional networks,” *CoRR*, vol. abs/1311.2901, 2013. [Online]. Available: <http://arxiv.org/abs/1311.2901> 3
- [41] C. Szegedy, V. Vanhoucke, S. J. Shlens, and Z. Wojna, “Rethinking the inception architecture for computer vision,” *CoRR*, vol. abs/1512.00567, 2015. [Online]. Available: <http://arxiv.org/abs/1512.00567> 3
- [42] O. Russakovsky, J. Deng, H. Su, J. Krause, S. Satheesh, S. Ma, Z. Huang, A. Karpathy, A. Khosla, M. Bernstein et al., “Imagenet large scale visual recognition challenge,” *International Journal of Computer Vision*, vol. 115, no. 3, pp. 211–252, 2015. 3, 4, 5, 9
- [43] L. v. d. Maaten and G. Hinton, “Visualizing data using t-sne,” *Journal of Machine Learning Research*, vol. 9, no. Nov, pp. 2579–2605, 2008. 6, 7
- [44] D. P. Kingma and J. Ba, “Adam: A method for stochastic optimization,” *CoRR*, vol. abs/1412.6980, 2014. [Online]. Available: <http://arxiv.org/abs/1412.6980> 5
- [45] R. Girshick, J. Donahue, T. Darrell, and J. Malik, “Rich feature hierarchies for accurate object detection and semantic segmentation,” in *Proceedings of the IEEE conference on computer vision and pattern recognition*, 2014, pp. 580–587. 7, 8, 10
- [46] K. He, X. Zhang, S. Ren, and J. Sun, “Spatial pyramid pooling in deep convolutional networks for visual recognition,” *CoRR*, vol. abs/1406.4729, 2014. [Online]. Available: <http://arxiv.org/abs/1406.4729> 7, 8
- [47] R. B. Girshick, “Fast R-CNN,” *CoRR*, vol. abs/1504.08083, 2015. [Online]. Available: <http://arxiv.org/abs/1504.08083> 7, 8, 10, 11
- [48] J. R. Uijlings, K. E. Van De Sande, T. Gevers, and A. W. Smeulders, “Selective search for object recognition,” *International journal of computer vision*, vol. 104, no. 2, pp. 154–171, 2013. 8
- [49] T. Lin, M. Maire, S. Belongie, J. Hays, P. Perona, D. Ramanan, P. Dollár, and C. L. Zitnick, *Microsoft COCO: Common Objects in Context*. Cham: Springer International Publishing, 2014, pp. 740–755. [Online]. Available: [http://dx.doi.org/10.1007/978-3-319-10602-1\\_48](http://dx.doi.org/10.1007/978-3-319-10602-1_48) 9
- [50] M. Everingham, L. Van Gool, C. K. Williams, J. Winn, and A. Zisserman, “The pascal visual object classes (voc) challenge,” *International journal of computer vision*, vol. 88, no. 2, pp. 303–338, 2010. 9

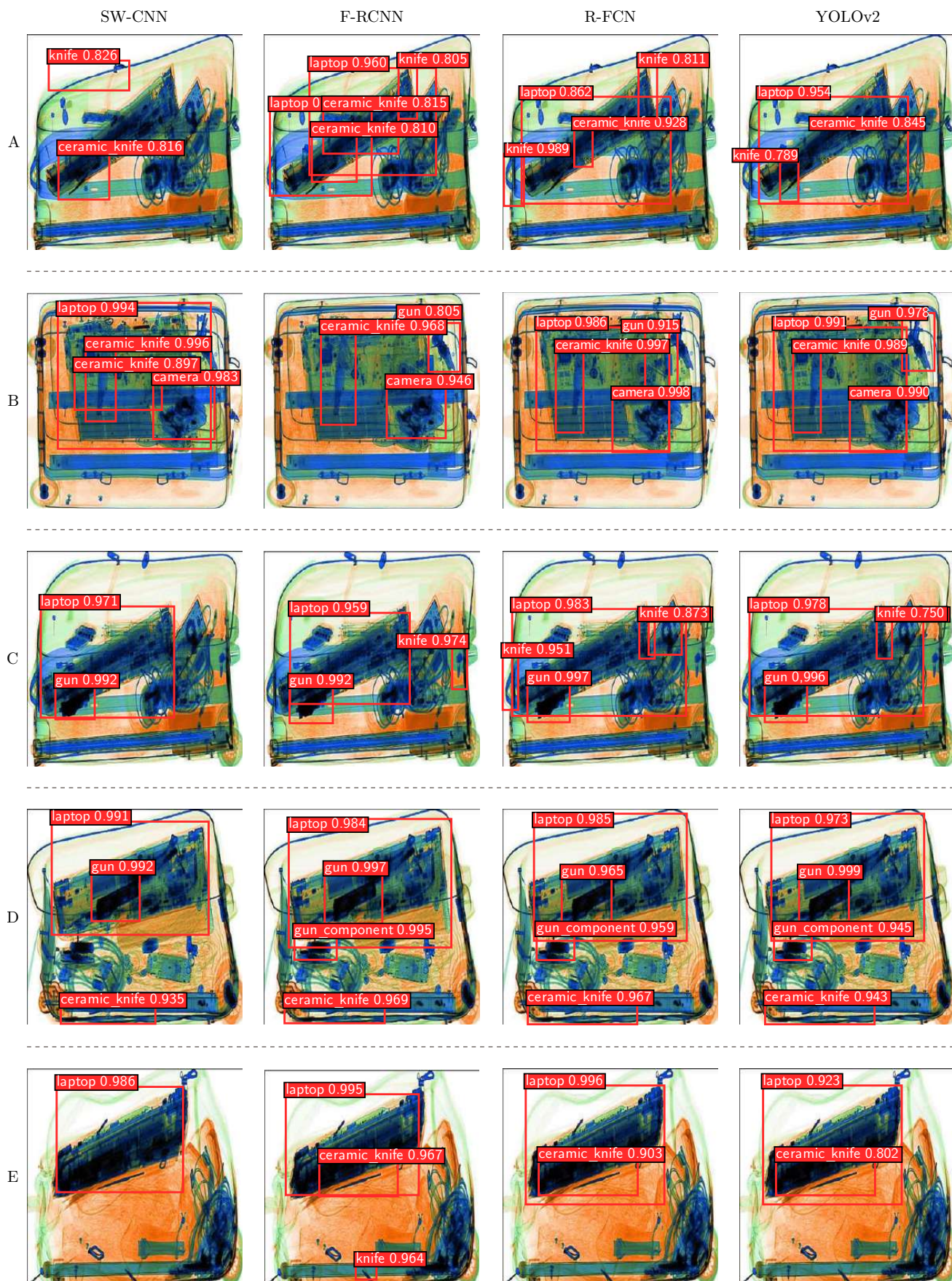


Fig. 10: Detection examples using ResNet<sub>101</sub>. Columns: SW-CNN, Faster RCNN, R-FCN and YOLOv2.